Carbon 142 (2019) 420–429

Contents lists available at ScienceDirect

Carbon

journal homepage: www.elsevier.com/locate/carbon

# Atomistically informed multiscale modeling of radially grown nanocomposite using a continuum damage mechanics approach

Karthik Rajan Venkatesan, Nithya Subramanian, Ashwin Rai, Aditi Chattopadhyay*

*School for Engineering of Matter, Transport, and Energy, Arizona State University, Tempe, AZ, 85281, USA*

ARTICLE INFO

*Article history:*
Received 15 August 2018
Received in revised form
13 October 2018
Accepted 16 October 2018
Available online 24 October 2018

ABSTRACT

An atomistically-informed multiscale modeling framework to investigate damage evolution and failure in radially-grown carbon nanotube (CNT) architecture is detailed in this paper. Molecular dynamics (MD) simulations are performed to investigate the effects of nano-reinforcements on the elastic-plastic characteristics of the constituent interphase in the radially-grown nanocomposite. An interphase damage model is developed using the continuum damage mechanics approach with damage evolution equations derived using atomistic simulations. The developed damage model is integrated with a high-fidelity micromechanical analysis and captures the underlying physical behavior that could be attributed to the enhancement of the out-of-plane properties at higher length scales. The mechanical properties of the nanocomposite obtained from micromechanical simulations are compared to experimental values reported in the literature, to validate the developed modeling framework. Conclusions are presented by comparing the material response of radially-grown CNT architectures with the traditional fiber reinforced polymer (FRP) with dispersed CNT architecture.

© 2018 Elsevier Ltd. All rights reserved.

## 1. Introduction

Recent advances in nanotechnology have led to the development of nano-engineered novel CNT architectures such as nano forests, radially-grown CNTs, and CNT ropes that have the potential to impact a wide range of applications through improved mechanical performance and adding new functionalities [1–3]. While these predefined CNT architectures have shown promising results in the transfer of nanoscale properties to the bulk structure [4,5], optimizing such architectures for significantly improved performance metrics remains a challenge. Their implementation is also limited due to the lack of complete understanding of the effects CNTs impart to the bulk properties of composites. A significant problem is the complex damage initiation and failure mechanisms, which are influenced by the inherent inhomogeneity of the material system and material and geometric variability. For predictive models to be accurate, an understanding of the underlying mechanics that govern the scalability of these materials, which includes possible changes in the fundamental properties of the host material when nanomaterials of different architectures are incorporated, as well as the benefits offered at higher length scales, is necessary [6,7].

Among the various predefined nanoarchitectures, the introduction of CNTs in fiber-reinforced polymer through CNT deposition/growth on the fiber has shown remarkable performance gains compared to the conventional strategies, such as CNT dispersion in the matrix. In radially-grown architecture, difficulties such as CNT agglomeration, filtration, and increased viscosity are avoided, and hence higher CNT concentrations can be achieved than when CNTs are dispersed in the matrix [8]. Consequently, several researchers are investigating the morphological and interfacial properties of radially-grown CNTs on fiber surface by characterizing properties such as surface area, fracture energy, interfacial shear strength (IFSS) and delamination. The incorporation of such nano-engineered architecture has shown up to a 60% increase in fiber/matrix interface strength [9,10] and a 33% improvement in impact toughness [11]. The transverse properties are also significantly improved compared to traditional CFRPs as reported in Ref. [12]. The increase in IFSS and modulus has been attributed to local stiffening and mechanical interlocking of the polymer at the fiber/matrix nano-engineered interphase [13,14]. Several studies have reported that the presence of CNTs in the fiber/matrix interphase region suppresses the stress concentration [12,15] and acts as an intermediate bridge that plays a significant role in load transfer

* Corresponding author.
*E-mail address:* aditi@asu.edu (A. Chattopadhyay).

https://doi.org/10.1016/j.carbon.2018.10.051
0008-6223/© 2018 Elsevier Ltd. All rights reserved.

mechanisms. Detailed experimental investigation of the interphase behavior can be challenging due to many physical variables and their complex interactions at various length scales. Therefore, there is a need for multiscale modeling methodologies that bridge the necessary length scales while capturing and modeling the fundamental phenomena at the critical length scales to predict damage and failure mechanisms in nano-engineered composite structures.

The properties of CNT-enhanced composites have been modeled in the past using approximation techniques such as the Mori-Tanaka formulations [16], composite cylinder assemblage [17], and effective properties approach [18]. These approaches are often not adequate as they fail to capture the stress state at the submicroscale and the molecular interactions at the nanoscale. The importance of modeling these phenomena to predict damage initiation in CNT-enhanced nanocomposites have recently been reported [19,20]. In radially-grown CNT architecture, the presence of CNT at the fiber/matrix interface creates a unique stress state at the nanoscale. Failure to capture this behavior at the submicroscale can lead to unreliable damage predictions. Several investigations have been carried out at the continuum scale to understand the load transfer and elastic behavior of radially-grown CNT nanocomposites using deterministic [21–23] and stochastic multiscale modeling techniques [24,25]. However, their implementation is limited due to the lack of complete understanding of the stress transfer characteristics and the interactions between various constituent interface/interphases along multiple length scales. Moreover, to the best of authors' knowledge, there is no reported work on modeling the physics associated with load transfer, architectural variability, and complex damage mechanisms in radially-grown CNT nanocomposites at multiple length scales.

This paper presents a multiscale modeling framework to characterize the interface between the fiber and matrix in radially-grown nanocomposites by integrating an atomistic model with a micromechanical model. In our previous work, an atomistic model of the CNT/fiber/matrix interphase region was developed to capture the unique response that could be attributed to improved out-of-plane nanocomposite properties [26]. Along the out-of-plane transverse direction, the interphase region exhibits a multi-stage deformation behavior, which combines complex phenomena such as plasticity, softening, rehardening, and failure mechanisms. It was also concluded that the failure in the critical interphase region is dominated by the mechanisms arising from loads transverse to the CNT growth direction. In this paper, the effect of varying CNT concentrations on the elastic-plastic and damage response of the nanocomposite interphase is evaluated through molecular dynamics simulations. An atomistically-informed continuum damage model with internal variables representing polymer mechanics and damage evolution for different CNT concentrations in the interphase is developed to accurately simulate the response and complicated damage process in radially-grown CNT architecture. The developed model in conjunction with the atomistically-informed damage model for thermoset polymers proposed by Rai et al. [27] is further applied to a radially-grown CNT nanocomposite repeating unit cell (RUC) within the high-fidelity generalized method of cells (HFGMC) micromechanics framework, while fiber failure is disregarded. Results show that the developed damage model can capture the unique stress-strain response in the interphase region observed at the nanoscale. The model provides insights into the underlying physical mechanisms that could be attributed to enhancement in out-of-plane properties at higher length scales. Furthermore, the performance and property gains from the radially-grown architecture are compared with traditional carbon fiber reinforced polymer composites (CFRP) with dispersed CNTs in the matrix at the micro length scales.

## 2. Molecular dynamics model

Molecular dynamics (MD) simulations are performed at the nanoscale to inform the continuum level HFGMC framework. The radially-grown nanocomposite model at the atomistic scale is originally comprised of five constituents: carbon fiber surface, polymeric functional coating (PSMA), radially-grown CNTs, the epoxy resin, and the crosslinker (see Fig. 1). The carbon fiber surface is simulated with void-induced, irregularly-stacked, graphene layers to simulate surface roughness; radially-grown CNTs are embedded in the PSMA chains; they are physically dispersed with no functionalization. The epoxy consists of DGEBF (Di-Glycidyl Ether of Bisphenol F) as the resin and DETA (Di-Ethylene Tri-Amine) as the crosslinker, before curing, dispersed randomly in the unit cell inside a predefined box. The unit cell dimensions are $40 \times 45 \times 35\ nm^3$. A detailed description of the model set up, choice of force fields, and epoxy crosslinking simulations can be found in our previous work [28]. The MD simulations for the radially-grown nanocomposite are performed with hybrid classical force fields, initially. The simulations implement periodic boundary conditions (PBCs) along the *y*- and *z*-directions. However, the assumption of PBCs is not appropriate along the *x*-direction due to a phase discontinuity (at the interphase). In this work, we focus on capturing the effect of CNT areal density (the number of CNTs per $nm^2$ of graphene layer) on the elastic, elastic-plastic and damage initiation characteristics of the fiber/matrix interphase with radially-grown CNTs. To achieve this, the molecular model is constructed with a fixed number of graphene sheets, PSMA and epoxy molecules. Radially-grown CNTs of chirality (10,10) are embedded in the PSMA chains that are physically dispersed with no functionalization. Due to the high computational costs incurred by large-scale molecular systems, the modeling of radially-grown CNTs that have heights in the order of microns is not feasible via MD simulations. Hence, the length of the CNT is chosen to be only ~10 nm. However, it is assumed that the relative fraction of the interphase region is of critical relevance and is used as an input to model the interphase at the higher length scale. The relative fraction is estimated as the ratio between the height of the CNT and

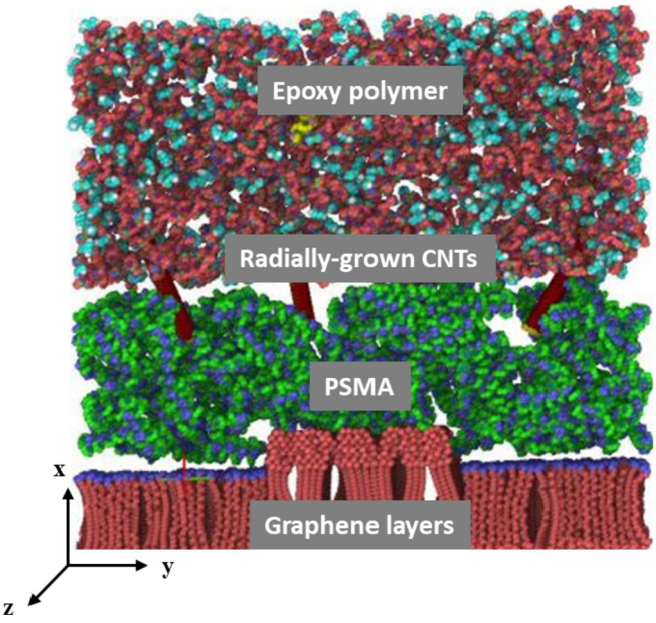


**Fig. 1.** Radially-grown CNT architecture interphase unit cell generated from PackMol [R]. (A colour version of this figure can be viewed online.)

thickness of the interphase (defined by the height of the unit cell) along the CNT growth direction. In this present atomistic model, the relative fraction of the interphase region is calculated to be ~0.25. The number of radially-grown CNTs is varied to capture a short range of areal densities. It should be noted that the upper limit of this range is dictated by the intermolecular forces of repulsion among the CNTs in the molecular system.

Equilibration and crosslinking MD simulations are performed first using classical force fields. The crystalline CNT and graphene molecules are defined by the Optimized Potential for Liquid Simulation – All Atom (OPLS-AA) [29] and the Consistent Valence Force Field (CVFF) [30]. The thermoplastic PSMA chains and the thermoset epoxy molecules utilize the Merck Molecular Force Field (MMFF) [31] parameters. The deformation MD simulations are performed using a reactive force field (ReaxFF) [32] that is capable of capturing bond elongation and bond scission events. A tensile load is applied to the molecular model by uniformly deforming the simulation box along the y-direction. The applied strain translates to the elongation of bonds causing the atoms to be remapped, and the equivalent stresses are obtained from the spatial and temporal averaging of virial stresses [33]. An ultra-high strain rate approach, as developed by Ref. [28], is employed to decouple thermal relaxation of bonds and capture the effect of bond elongation and breakage purely based on mechanical deformation. Therefore, the obtained response is a quasi-continuum-equivalent deformation of the molecular system. The variation of bond energy between the unbound state of the molecular model at the initial time step and at each time step of the simulation is used to calculate the bond dissociation energy. As deformation occurs, the bond energy lost due to dissociation of each covalent bonds in the system is calculated and defined as BDE. Further details of the boundary conditions and accompanying justifications are provided in Ref. [26].

It was concluded from our previous atomistic models of the radially-grown CNT fiber interphase that failure of this region is dominated by the mechanisms arising from loads transverse to the CNT growth direction (*y*-direction in the atomistic model in Fig. 1). These observations were justified by comparing the obtained maximum value of bond dissociation energy and the respective failure strains for different loading directions. A significant hypothesis that emerged subsequently was that, while the elastic behavior along *y*-direction was due to loads being transferred through polymer chain stretching, the CNTs reorient themselves to fill the voids caused by polymer chain extension. This reorientation of CNTs happens along the loading direction; as a result, strain-hardening tendencies were observed beyond the elastic regime. Further information on the MD model and the nanoscale stress-strain response curves can be found in Ref. [34]. Fig. 2 illustrates the smoothed elastoplastic stress-strain response obtained from virtual deformation simulations conducted for different CNT areal densities. In the elastic regime, the polymer chains in the interphase region are stretched along the direction of applied stress. In the yielding regime, the molecular configuration deforms and rearranges irreversibly. After yield, strain softening occurs due to the breakage of polymer chains due to successive bond dissociation. When strain softening is complete, strain hardening behavior emerges as a result of the subsequent realignment of CNTs along the loading direction in the newly generated voids. In the failure regime, the spacing between the CNT and the matrix increases, contributing to a secondary softening regime that leads to complete failure of the interphase material. This phenomenon cannot be determined and verified experimentally; however, the simulations provide insights into crucial nanoscale trends while considering the local interactions between the CNT, graphene layers and polymer matrix and influence of different CNT areal densities.

In our previous study, a molecular system with randomly distributed CNTs was generated to investigate the effect of nano-inclusions by weight fractions on the polymer cross-linking formation [35]. It was observed and quantitatively shown that the increase in CNT weight fraction reduced the mean crosslinking degree in the polymer. However, the gradient of reduction in crosslinking degree reduced at a much higher weight fraction due to the formation of CNT clusters causing localized highly cross-linked polymer regions. This formed the basis of the interpretation that the presence of CNTs interferes with the crosslink formation between the resin and the hardener molecules. In the present radially-grown CNT architecture, a similar reduction in the polymer crosslinking degree is observed with increase in CNT areal density. Therefore, the increase in CNT areal density in the interphase region results in a considerable decrease in the transverse elastic modulus. However, the slope of the hardening phase in the stress-strain curve increases with an increase in the areal density. Fig. 3 plots the associated bond dissociation energy (BDE) variation during the deformation simulations transverse to the CNT growth direction for varying CNT areal densities. The slope of the BDE curve with respect to strain is an indication of how much energy is expended for bond

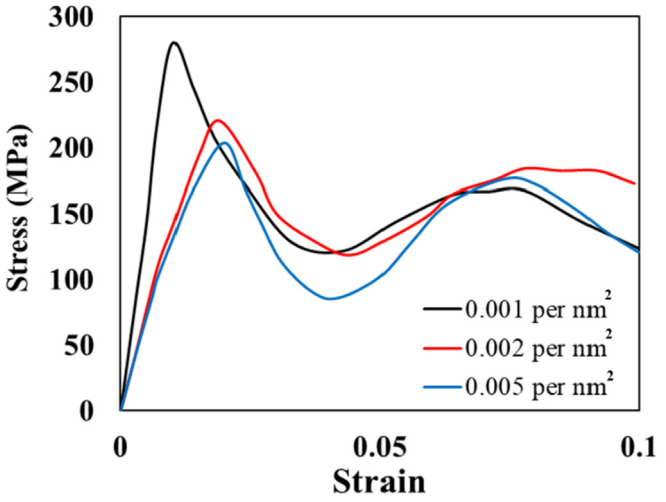


**Fig. 2.** MD model stress-strain response for radially-grown interphase with different CNT areal densities. (A colour version of this figure can be viewed online.)

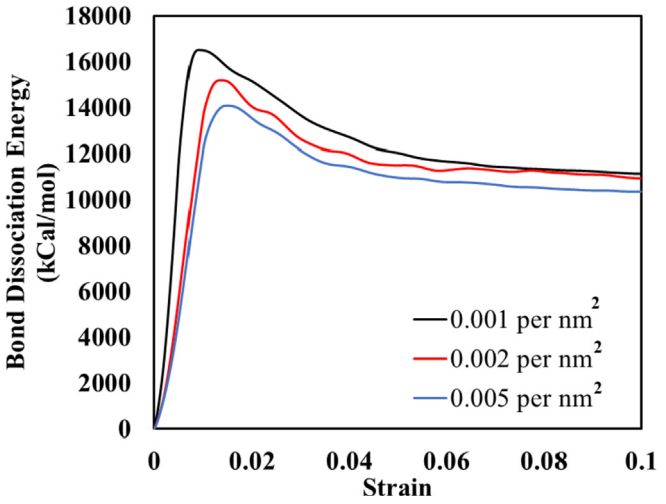


**Fig. 3.** MD model BDE curve for radially-grown interphase with different CNT areal densities. (A colour version of this figure can be viewed online.)

breakage from the applied deformation. The initial increase in the slope of the BDE curve up to ~2% strain indicates that the bond energy is lost due to the stretching and scission of low strength $sp^3$ bonds. After the failure of the polymer phase, the BDE curve saturates beyond ~4% strain, and the slope drastically reduces as a result of load transfer to the radially-grown CNTs. It is important to note that the rate of damage saturation (bond dissociation) increases with an increase in the areal density and leads to a prominent increase in the hardening phase. These nanoscale physical phenomena that are unique to radially-grown CNT architectures could be attributed to the increase in strength and toughness properties at higher length scales. The obtained stress-strain response and bond dissociation energy (BDE) variation which provide vital insights into these damage mechanisms are used as input to derive constitutive equations in the microscale continuum damage model described in the next section.

## 3. Constitutive material model

Motivated by the previous molecular dynamics results, it is necessary to accurately model the complex damage saturation and prominent strain hardening mechanism in the radially-grown CNT architecture. A constitutive material model for the interphase region is developed based on the continuum damage mechanics (CDM) framework, with damage evolution equations that are developed from elastoplastic MD simulations results. Firstly, the interphase region is modeled as an orthotropic material. Fig. 4(a) shows the local coordinate system which is defined by the fiber inclusion in the $x_1$ direction and the radially oriented CNTs in the orthotropic material frame ($x_2$-$x_3$). The six independent elastic parameters in the orthotropic material are obtained from the tensile and shear deformation MD simulations of the atomistic interphase model described in the previous section. The three independent Poisson's ratios are carefully estimated to ensure a positive-definite symmetric elasticity tensor $C_{ijkl}$.

In the CDM framework, constitutive equations and evolution laws of state variables are derived from the damage-coupled energy potentials. In the present study, based on the hypothesis of decoupling between elastic-damage and plastic hardening [36], the Helmholtz free energy density is expressed as

$$\psi = \psi_e\left(\varepsilon^e_{ij}, D_{ij}\right) + \psi_p(\xi, T) \tag{1}$$

where $\psi_e(\varepsilon^e, D)$ is a coupled damage-elastic strain energy and $\psi_p(\xi, T)$ is the free energy contribution due to plastic strain hardening, $\varepsilon^e_{ij}$ is the elastic strain tensor, $\xi$ is an internal variable representing the equivalent plastic strain $\bar{\varepsilon}^p$, $T$ is the temperature and the tensor $D_{ij}$ is the internal variable associated with damage.

With the additive decomposition of the strain rate $\dot{\varepsilon} = \dot{\varepsilon^e} + \dot{\varepsilon^p}$ and using the Clausius-Duhem inequality under isothermal conditions [37], the following relation can be obtained.

$$\gamma = \sigma : \dot{\varepsilon}^p - \frac{\delta\psi_e}{\delta D}\dot{D} - \frac{\delta\psi_p}{\delta\bar{\varepsilon}^p}\dot{\bar{\varepsilon}}^p \geq 0 \tag{2}$$

where $\gamma$ is the power of dissipation. The thermodynamic conjugate forces corresponding to the internal variables are derived from the free energy term and are expressed as

$$\sigma_{ij} = \frac{\delta\psi}{\delta\varepsilon^e_{ij}} = C_{ijkl}\varepsilon^e_{kl}, \tag{3}$$

$$Y_{ij} = -\frac{\delta\psi}{\delta D_{ij}} = \frac{1}{2}\varepsilon^e_{kl}\frac{\delta C_{klpq}}{\delta D_{ij}}\varepsilon^e_{pq} \tag{4}$$

$$\kappa = \frac{\delta\psi}{\delta\bar{\varepsilon}^p} \tag{5}$$

where $\sigma$, $Y$ and $\kappa$ are the thermodynamic affinities associated with the elastic strain $\varepsilon^e$, damage $D$ and the plastic strain due to molecular rearrangement in the polymer $\varepsilon^p$ respectively.

### 3.1. Constitutive equations

Using strain equivalence principle and assuming damage components in each direction evolve independently, the following relation for the coupled elastic-damage strain energy term can be obtained.

$$\psi_e = \frac{1}{2}\varepsilon^e_{ij}(1 - D_{ij})C_{ijkl}\varepsilon^e_{kl} \tag{6}$$

By substituting the strain energy expression from Eq. (6) in Eq. (3), the coupled elastic-damage law can be expressed as follows.

$$\sigma_{ij} = (1 - D_{ij})C_{ijkl}\varepsilon^e_{kl} \tag{7}$$

It is important to note that in the present work, the primary goal is to capture specific nano and sub-microscale features that could be attributed to the enhancement in out-of-plane properties of radially-grown nanocomposites. As observed from atomistic simulations, interphase failure under transverse loading is more predominant compared to the deformation behavior along the direction longitudinal to the CNTs. Along the transverse direction, the interphase region exhibits complex mechanisms such as plasticity, damage-softening, rehardening, and failure. Fig. 4(b) illustrates the various stages of deformation under transverse loading and the damage variable $D_2$, characterizes the corresponding damage evolution as shown in Fig. 5. Along the $x_3$-direction, the absence of a matrix-dominated softening mechanism is attributed to the load carrying role dominated by the graphene layers. Therefore, the interphase deformation along this direction is assumed to be linearly elastic. Consequently, a thermodynamically consistent model is implemented by defining a yield function to initiate failure along the transverse ($x_2$) direction as follows.

$$\varphi_p = \frac{\sigma^*_{eq}}{1 - D_2} - \sigma_{y_0} - \kappa \leq 0 \tag{8}$$

where $\sigma_{y_o}$ represents the yield stress in the referent direction, $\sigma_{eq}$ is the equivalent stress, and $\kappa$ is a scalar thermodynamic force associated with the plastic strain hardening, characterizing the expansion of the yield surface. A nonlinear plastic strain hardening free energy term is assumed and can be written as

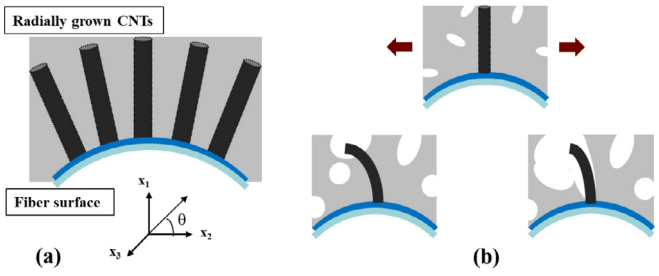


**Fig. 4.** (a) Local coordinate system of radially-grown CNT nanocomposite interphase; (b) different stages of deformation under transverse loading. (A colour version of this figure can be viewed online.)

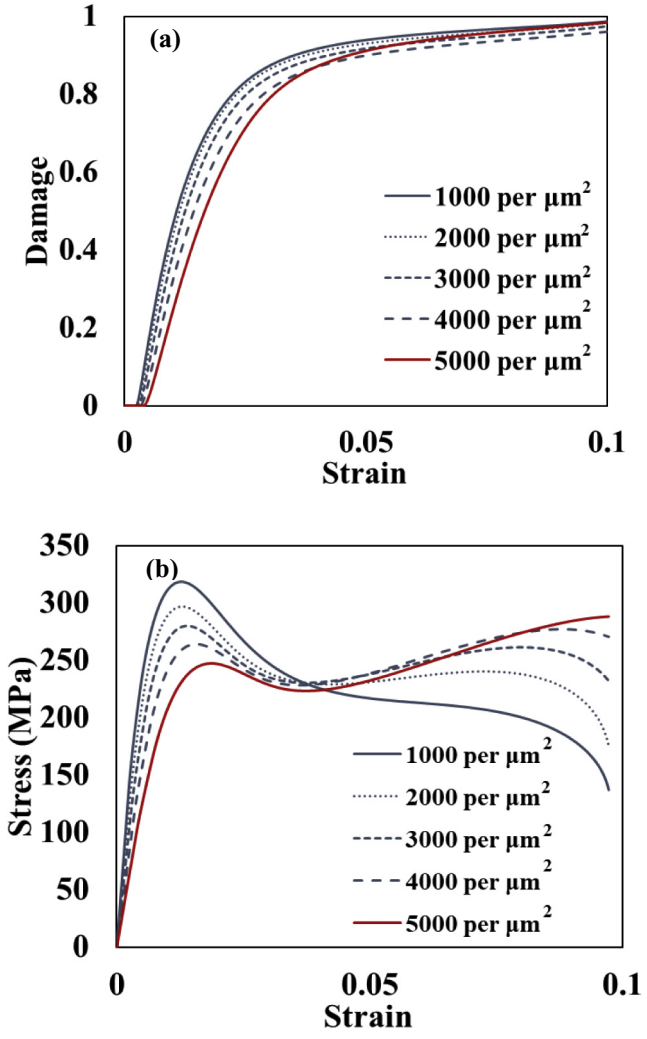


**Fig. 5.** Simulated interphase response for varying CNT areal density: (a) cumulative transverse damage evolution with applied strain; (b) corresponding stress-strain response. (A colour version of this figure can be viewed online.)

$$\psi_p = C_h(\bar{\varepsilon}^p)^{\gamma} \tag{9}$$

where $C_h$ and $\gamma$ are the hardening modulus and hardening index that represents the internal stresses developed by the polymer chain rearrangement and the subsequent realignment of CNTs along the loading direction. Substituting the above free energy term in Eq. (5), the thermodynamic force associated with hardening is obtained as

$$\kappa = \gamma C_h(\bar{\varepsilon}^p)^{\gamma-1} \tag{10}$$

Under the associative flow, the stress function defined in Eq. (8) acts as a yield function as well as plastic potential. With negligible plastic deformation along the $x_1$-and $x_3$-direction, the plastic strain evolution equation in the $x_2$-direction is obtained using the classical plasticity conditions and can be expressed as

$$\dot{\varepsilon}^p_{ij} = \dot{\lambda}\frac{\delta\varphi_p}{\delta\sigma_{ij}} = \frac{\dot{\lambda}}{1-D_2}\frac{\delta\sigma_{eq}}{\delta\sigma_{ij}} \tag{11}$$

where $\dot{\lambda}$ represents the viscoplasticity multiplier and is described in Ref. [38].

$$\dot{\lambda} = \frac{1}{K_v}\left[\left(\frac{\varphi_p + \sigma_{y_0}}{\sigma_{y_0}}\right)^{\frac{1}{\mu}} - 1\right] \tag{12}$$

where $K_v$ and $\mu$ are viscoplastic constants.

### 3.2. Damage evolution

The nanoscale mechanics of the interphase region derived using MD simulations, show that the CNT areal density governs the out-of-plane properties of radially-grown nanocomposites. At the continuum scale, the CNT areal density is defined as the number of CNTs grafted or grown per $\mu m^2$ of the fiber surface. Along the transverse direction, the post-yield softening and strain hardening behavior are mainly due to the polymer bond breakage, molecular rearrangement and consequent reorientation of CNTs at the nanoscale. In the present formulation, a damage evolution equation based on BDE variation is developed to surrogate the nanoscale damage kinetics in the CNT reinforced interphase region.

To model the proposed multi-stage deformation behavior illustrated in Fig. 4(b), a damage variable $D_2$ is introduced to characterize the corresponding damage evolution along the y-direction. Two distinct softening variables are introduced to account for the dual softening behavior observed in the MD simulations. The BDE variation shown in Fig. 3(a) is used to model the evolution of the primary damage variable $D_s$. It is important to note that the calculated BDE variation from the MD simulations shown in Fig. 3(a) plots the instantaneous difference in bond energy due to the breakage of covalent bonds in the system. The calculated variation accounts only for the bond breakage and does not consider the cumulative variation of bond breakage energy being converted to non-bonded pair energy interactions. A damage saturation law is assumed to characterize $D_s$ and the point of damage saturation is calibrated from the BDE curve for the value of strain at which the BDE begins to saturate. The evolution of the secondary damage variable $D_f$ is developed to simply surrogate the final drop in the stress-strain curve obtained from the MD simulations. The atomistic interphase model shows a considerable decrease in transverse modulus with an increase in areal density. This behavior is ascribed to the increase in local stress concentrations in the polymer due to the increase in the volume concentration of CNTs. However, the rate of damage saturation and hardening mechanism are more prominent with increased areal density. Hence, the damage evolution equation is developed to reflect this change of nature of damage with a change in CNT areal density and is expressed as

$$\dot{D}_s = \frac{\dot{\lambda}}{2}\left(\frac{(1+\alpha) - D_s\rho^{\eta}}{\rho^{\eta}}\right)Y^{\xi} \tag{13}$$

$$\xi = \alpha\rho^{\eta} \tag{14}$$

where $\rho$ is the CNT areal density, $\alpha$ is a phenomenological constant associated with the damage saturation when the realignment of CNTs is complete and $\eta$ is the rate of damage growth. To capture the dual softening behavior, a secondary damage variable, also called the failure variable, is obtained as

$$\dot{D}_f = \frac{\dot{\lambda}}{2}\left(\frac{Y}{Y_0\sqrt{1-D_f}}\right) \tag{15}$$

where $Y_0$ is a material parameter associated with the slope of the secondary softening curve. The variation of damage evolution versus applied strain shown in Fig. 5(a) gives the combined

response of the two-distinct damage variable, which contributes to the dual softening stress-strain response. As a validation process, the combined damage response is compared with the cumulative BDE variation obtained from a recent publication by the authors [26]. Fig. 6 (a) shows the obtained BDE variation as a function of the applied strain for a CNT areal density of ~0.003 per nm$^2$. It should be noted that this BDE variation is calculated by considering energy due to bond breakage and the non-bonded pair energy variations which gives the cumulative variation of the deformation response. Fig. 6 (b) shows the normalized BDE variation and the damage evolution for a CNT areal density of ~0.003 per nm$^2$. The predicted cumulative damage evolution shows good correlation with the normalized cumulative BDE variation. It is important to note that the assumed damage evolution equation is based on an exponential saturation law while the obtained BDE curve shows a highly non-linear response. It is also worth mentioning that key characteristics such as change in gradient and damage saturation are sufficiently captured by the developed damage evolution model. The variation of stress-strain response with CNT areal density is shown in Fig. 5(b). At high CNT density, the model predicts improved damage saturation and a more prominent hardening behavior as compared to lower CNT density where the stiffness improves. The change in gradient and slope of the damage curve are the key features of interests are sufficiently captured by the developed damage evolution model.

The developed constitutive model considers the variation of material behavior with CNT density in the direction transverse to the radially-grown CNTs. Hence, a relationship between transverse yield strength and CNT density, $\rho$, is derived through molecular dynamics simulations. The yield point is computed using MD simulations with appropriate force fields as described in the previous section. From the simulation results, the yield strength for a range of CNT areal density was calculated using virtual deformation tests along the $x_2$-direction. The linear fit model was found to have the following form.

$$\sigma_{y_o} = 135.5 - 0.0076\rho \tag{16}$$

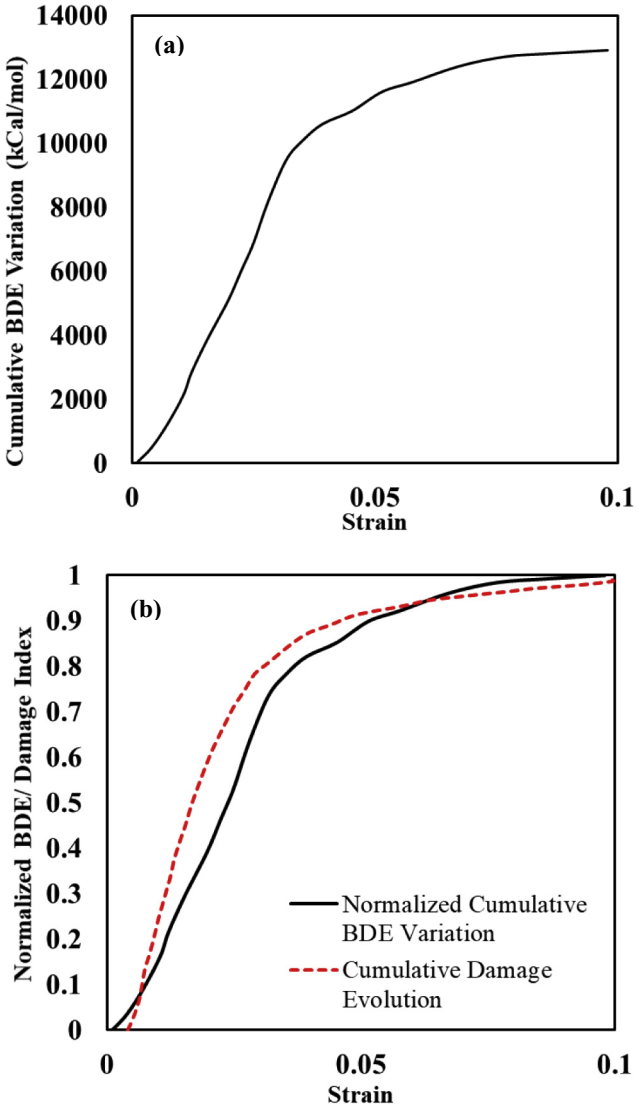


**Fig. 6.** Comparison of the BDE variation with cumulative damage evolution for a CNT areal density of ~0.003 per nm$^2$: (a) Cumulative BDE variation with applied strain [33]; (b) Comparison of normalized BDE with cumulative damage obtained using the interphase model. (A colour version of this figure can be viewed online.)

## 4. Micromechanical model

Previously, it is observed that the CNT areal density in the interphase region affects the out-of-plane properties significantly. Therefore, the local fiber/matrix interphase region is modeled at the micro length scale to quantify the influence of the CNT areal density on the global response of radially-grown nanocomposite. Firstly, the HFGMC based micromechanics theory is employed to model the nanocomposite microstructure with repeating unit cell consisting of fibers reinforced in a polymer matrix. The unit cell is assumed to be periodically distributed in the $y_2 - y_3$ plane and is discretized into $N_\beta$ and $N_\gamma$ subcells along the $y_2$-direction (height) and $y_3$-direction (width). The composite unit cell is defined by a continuous fiber inclusion in the $y_1$-direction. Hence, the computational costs of the framework are reduced by setting the unit cell thickness in the fiber direction to one subcell thick. The critical interphase region in the radially-grown CNT architecture is modeled with interphase subcells that are adjacent to the fiber subcells as illustrated in Fig. 5. In an ideal case, the interphase subcells can be considered cylindrically orthotropic with $\theta \in [0, 2\pi]$ as the angle formed by the in-plane direction of the nanoscale RVE to the axis of the corresponding fiber as shown in Fig. 7.

The strain transformation matrix $T_\varepsilon$ can describe the relationship between the interphase subcell coordinate system and the microscale coordinate system. The elastic properties determined from the atomistic simulations of the interphase region are incorporated into the micromechanical model of interphase subcells using the transformation matrix and is expressed as

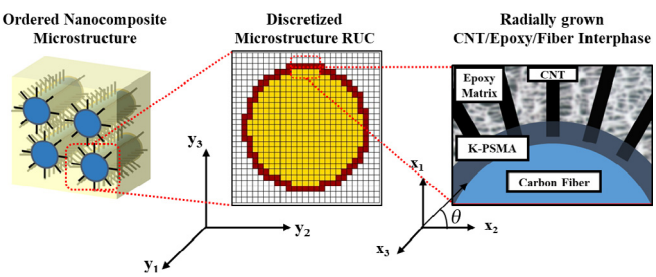


**Fig. 7.** Schematic representation of the repeating unit cell (RUC) with the polymer (white), fiber (yellow) and interphase (red) subcells. (A colour version of this figure can be viewed online.)

$$\overline{C}_{int} = T_{\varepsilon} C_{int} T_{\varepsilon}^{T} \tag{17}$$

where the subscript 'int' denotes interphase.

A geometrical relationship is derived to estimate the average CNT volume fraction $V_{cnt}$ at the microstructure level as a function of the CNT areal density at the sub-microscale.

$$V_{cnt}(\%) = \sum_{n=1}^{N_f} \left( \frac{\rho \pi d_{cnt}^2 t_{int}}{D} V_f \cdot n \right) \times 100 \tag{18}$$

where $D$, $N_f$ and $V_f$ are the diameter, number of fibers and volume fraction of the fiber in the RUC, $d_{cnt}$ is the diameter of radially-grown CNTs, and $\rho$ is the CNT areal density at the sub-microscale. The parameter $t_{cnt}$ characterizes the thickness of the CNT-enhanced fiber/matrix interphase region. Several experimental studies suggest that the presence of radially-grown CNT leads to local stiffening of the epoxy at the interphase region [13–15]. Simulation studies shows that relatively short (~500 nm) and dense CNTs enhances the stresses in the matrix due to stress concentrations shifting from the interphase region towards the ends of CNTs [39]. This formed the basis of our premise that the presence of CNT in the fiber/matrix interface has an extended reinforcing effect beyond the ends of CNTs. Hence, it is assumed that the thickness of the interphase region $t_{cnt}$ can adequately capture the experimentally observed reinforcing effect and is primarily dictated by the relative fraction estimated from the atomistic model discussed in section 2. Fig. 8 shows the variation of CNT volume fraction with respect to the number of CNTs grown per $\mu m^2$ on a single fiber at 40% volume fraction of fiber for normalized unit thickness of the interphase region.

The HFGMC micromechanics theory employs a higher-order subcell displacement field which enables shear coupling between neighboring subcells. As a result, the current framework can accurately capture the effect of the interphase properties on the nanocomposite response. The solution procedure for the displacement field is detailed in Ref. [40]. Each subcell in the RUC is assigned material properties and a constitutive law to describe the local behavior. The constitutive equations for the fiber subcells are defined with a transversely isotropic, linear elastic constitutive law,

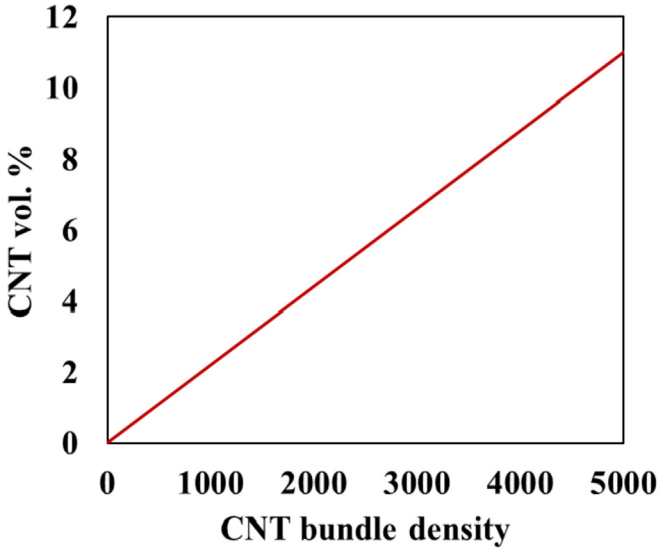


**Fig. 8.** CNT volume concentration at the microscale as a function of CNT areal density at the nanoscale. (A colour version of this figure can be viewed online.)

while the polymer subcells are defined as isotropic material. The isolated effects of the local PSMA coating in the interphase region are not considered in this study. The damage model for the radially-grown CNT nanocomposite interphase, described in the previous section, in conjunction with the atomistically informed damage model for thermoset polymers [41] is further applied to the RVE within the HFGMC framework.

## 5. Results of HFGMC simulations

This section presents results and predictions from the atomistic interphase damage model applied to the high-fidelity micromechanical model. The present modeling framework is validated by comparing the elastic mechanical properties of unidirectional radially-grown CNT nanocomposite (2% CNT volume fraction) with experimental data from the literature [42,43]. As stated in Ref. [42], CNTs with diameter d = 30 nm, height $h$ = 100 nm, and a volume fraction of 2% were radially grown on fiber surface of diameter D = 5.2 μm. It should be noted that the height of the CNTs in experiments is higher compared to the height of the CNTs used in the atomistic simulations. As previously stated, the effect of the CNT-reinforced interphase region is assumed to extend over a certain height. Hence, the relative fraction (~0.25) obtained from the atomistic model is used as a rough measure to estimate the thickness of the reinforced interphase region associated with the height of radially-grown CNTs. As a result, the predicted value of the transverse modulus matches well with the test data when the thickness of the interphase region is estimated to be ~800 nm that is equivalent to ~200 nm in the height of the CNTs. Although the value is merely estimated to match the experimental data, detailed investigation on the effect of the thickness of the interphase region is needed to fully understand the underlying physical association and adequately model the effect of the CNT-reinforcements. It should be noted that an areal density of $10^3$ CNTs per $\mu m^2$ is chosen to model the nanocomposite with ~2% CNT volume fraction.

As shown in Table 1, the predicted longitudinal and transverse modulus obtained from the HFGMC model are in good agreement with the experimental observations. The predicted elastic response of radially-grown nanocomposite yields up to a 21.3% improvement in the transverse modulus with respect to traditional fiber reinforced composites as shown in Table 1. However, the longitudinal modulus of the composite deteriorates in the presence of heterogeneous interphase region. This degradation could be attributed to the interphase region acting as surface defects on the fiber, thereby degrading the load transfer characteristics along the fiber direction.

### 5.1. Damage simulation for transverse tensile loading

The influence of matrix cracking on the transverse fracture behavior is captured using the atomistically-informed damage model for thermoset polymers simulated at 60% crosslinking degree. The effect of fiber/matrix interphase failure in radially-grown CNT architecture is examined using the developed atomistically-informed interphase damage model. The variation of the transverse stress-strain response of the nanocomposite with CNT areal density is plotted in Fig. 9. The increase in areal density shows no significant variation in the transverse elastic modulus. In general, the increase in areal density or CNT volume fraction is expected to improve the modulus of elasticity in the out-of-plane direction. The authors hypothesize that this discrepancy could be due to variations in elastic modulus of the interphase region along the direction of CNTs, which is not considered in this study. However, the nanocomposite with low CNT areal density fails early due to the interphase cracks, and the transverse tensile strength is lowest. The nanocomposite at higher areal density shows higher transverse

**Table 1**
Comparison between experimental data and atomistically-informed microscale model for 2% CNT vol. fraction.

| | Atomistically-informed HFGMC | | Experimental data | |
|---|---|---|---|---|
| | $E_{11}$ (GPa) | $E_{22}$ (GPa) | $E_{11}$ (GPa) | $E_{22}$ (GPa) |
| CFRP w/radially-grown CNT | 187[a] | 10.01[b] | 203 ± 7.6[a] [43] | 10.02 ± 1.13[b] [42] |
| CFRP | 189.33[a] | 8.25[b] | 198.3 ± 5.0[a] [43] | 7.8 ± 1.09[b] [44] |

[a] 70% Fiber Volume Fraction.
[b] 40% Fiber Volume Fraction.

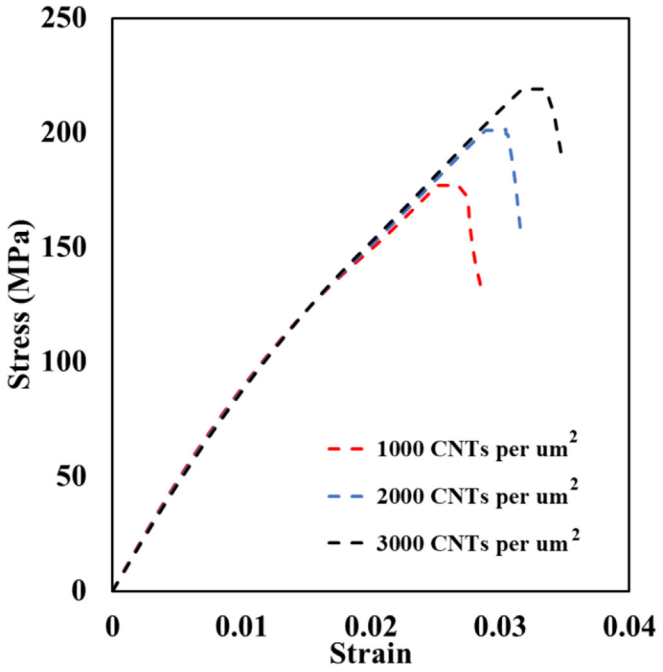


**Fig. 9.** Micromechanical model predictions for the transverse failure response of radially-grown CNT nanocomposite for varying CNT areal density. (A colour version of this figure can be viewed online.)

strength properties. This is attributed to the nanoscale phenomena where the increased number of radially-grown CNTs leads to improved damage saturation of the polymer matrix in the interphase region. Also, the increase in areal density causes a more substantial strain softening region with a higher strain to failure. The energy absorption capabilities, as determined by the area under the stress-strain curve, improve with the increase in CNT areal density. This improvement is attributed to the prominent strain hardening tendencies associated with the reorientation of CNTs along the loading direction at the nanoscale.

### 5.2. Effect of nano-engineered architecture

This sub-section investigates the effect of nano-engineered architecture using the developed atomistically-informed high-fidelity micromechanical model. The effect of radially-grown CNT architecture is compared with traditional CNT-enhanced carbon fiber reinforced composites to investigate the load transfer characteristics and the isolated influence of matrix cracking on the transverse material response. As a case study for microstructural analysis, the microscale RUCs with CFRP composite containing a CNT-enhanced polymer, and radially-grown CNT with 2% volume fraction of CNTs and 40% volume fraction of fiber are generated. In the case of the RUC with dispersed CNT-CFRP, the elastic properties of the nanopolymer are obtained from our previous established modeling framework for CNT-enhanced nanopolymer systems [35]. The dispersion of CNT in the polymer phase was found to interfere with the polymer crosslinking degree. The model predictions showed that the average cross-linking degree (CLD) was found to be 66.32% at ~0% CNT volume fraction, and 47.14% at ~2% CNT volume fraction in the polymer phase. The corresponding cross-linking degree values are used in the atomistically-informed damage model for thermoset polymers to obtain a reliable comparison between the two CNT architectures and the influence of matrix cracking on the transverse progressive damage response, while the fiber/matrix interphase failure or debonding is disregarded. These unit cells are subjected to boundary conditions corresponding to the deformation along the direction transverse to the fiber. The specific material properties and parameters used in the interphase constitutive model are detailed in Table 2. The material properties used for the fiber and matrix phase are detailed in Table 3.

Fig. 10 compares the transverse stress-strain response of the radially-grown CNT-CFRP with traditional CFRP composites containing a neat polymer and CNT-enhanced nanopolymer. The micromechanical model predicts significantly improved stiffness and load transfer characteristics in radially-grown architecture compared to traditional CFRP composites with neat polymer while slightly lower stiffness when compared to CFRP with CNT-enhanced nanopolymer. However, the radially grown CNT architecture displays delayed onset and slower propagation of matrix damage compared to the CFRP with dispersed CNT in the polymer. This observation associates well with existing literature findings [45] where radially-grown CNT architectures showed better fracture properties than traditional CFRP composites with neat polymer and CNTs dispersed in nanopolymer. These improvements in the radially-grown architecture are attributed to the presence of CNT enhanced interphase region, which plays an essential role in the redistribution of stresses in the matrix around the fiber. The radially grown architecture leads to superior interfacial interactions between the CNTs and the host matrix resulting in efficient load transfer to the radially-grown CNT reinforcements. The increase in CNT volume fraction (or CNT areal density) leads to increased transverse strength and energy absorption properties, which in turn could lead to improved interlaminar shear strength and impact toughness at higher length scales.

On the other hand, the CFRP composite with CNT dispersion in the matrix leads to a noticeable increase in energy absorption compared to traditional CFRP with the neat polymer. However, dispersed CNTs in nanopolymer tends to interfere with the polymer cross-linking degree, and often agglomerate and form clusters at higher volume fractions. This phenomenon significantly affects the load transfer between the CNTs and the matrix and accelerates the damage propagation in the matrix phase. Therefore, the traditional CFRP composites with dispersed CNT architecture does not take advantage of the unique properties of the CNTs, thereby leading to inferior properties at higher volume concentrations of CNT. Whereas the property enhancements in radially-grown nanocomposite can be ascribed to be one of the unique architectural

**Table 2**
Material model parameters for radially-grown interphase region.

| Elastic Properties | | Model Parameters | | | |
|---|---|---|---|---|---|
| $E_1$ | 17.32 GPa | $\rho$ | $10^3$ CNTs/$\mu m^2$ | $Y_0$ | 0.04 GPa |
| $E_2$ | 15.39 GPa | $\eta$ | 0.042 | $t_{int}$ | ~800 nm |
| $E_3$ | 27.61 GPa | $C_h$ | 5 GPa | | |
| $G_{32}$ | 2.35 GPa | $\mu$ | 1.5 | | |
| $G_{21}$ | 4.58 GPa | $K_v$ | 0.6 | | |
| $G_{13}$ | 3.16 GPa | $\alpha$ | 0.20 | | |

**Table 3**
Material properties of fiber and matrix phase.

| Properties of IM7 Carbon Fiber | | Properties of Neat Epoxy | | Properties of Epoxy with Dispersed CNTs | |
|---|---|---|---|---|---|
| $E_1$ | 294 GPa | $E$ | 2.61 GPa | $E$ | 4.41 GPa |
| $E_2, E_3$ | 18.5 GPa | $\nu$ | 0.35 | $\nu$ | 0.41 |
| $\nu_{23}$ | 0.30 | $\eta$ (CLD) | 66.32% | $\eta$ | 47.14% |
| $\nu_{12}$ | 0.27 | | | $V_{cnt}$ | ~2% |
| $G_{23}$ | 25 GPa | | | | |

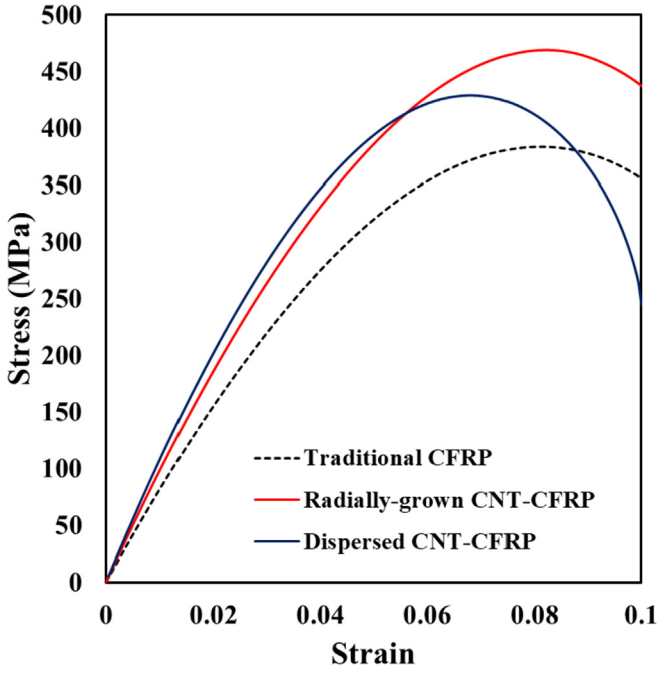


**Fig. 10.** Micromechanical model predictions for the transverse response of radially-grown CNT (2% CNT volume fraction) and traditional CFRP composite. (A colour version of this figure can be viewed online.)

benefits that provide exceptional performance gains at a higher volume concentration of CNT.

## 6. Conclusions

The significance of radially-grown nanoarchitecture was highlighted in this paper, in addition to the development of a multiscale modeling framework that can accelerate the development and optimization of such novel architectures. The nanoscale mechanics in the radially-grown CNT configuration have been modeled using MD simulations to investigate the effect of CNTs in the fiber/matrix interphase region. A previously developed atomistic model of the radially-grown nanocomposite was used to investigate the effect of CNT concentrations in the interphase region. The damage and failure mechanisms were found to vary based on the CNT areal density in the heterogeneous region. The out-of-plane elastic modulus decreased with increase in areal density. However, the failure mechanisms improved significantly with an increase in the areal density. The BDE variation was obtained as a function of strain, which provided vital insights into the damage mechanisms along the direction transverse to the CNT growth. The nano-engineered interphase region in radially-grown architecture was modeled as orthotropic fiber/matrix interphase subcells using the HFGMC framework. The obtained elastic response of the radially-grown nanocomposite correlates well with available experimental data, establishing the validity of the present approach using atomistically informed interphase subcell properties. A CDM-based constitutive model was developed using the variation in BDE obtained from MD simulations to accurately simulate the damage mechanisms in the heterogeneous interphase region. The developed interphase damage model was integrated within a high-fidelity micromechanical framework to investigate the transverse failure response of radially-grown nanocomposites. The nanocomposite with higher CNT areal density showed higher transverse strength and a larger strain-softening region at the micro length scale, indicating possible improvements in the interlaminar strength and energy absorption properties at higher length scales. Finally, a case study was conducted to investigate the load transfer, and damage initiation, and propagation in traditional CFRP composites with dispersed CNT and radially-grown CNT architecture at the micro length scale. The microscale RUC with radially grown CNTs showed significant improvements in the load transfer behavior and delayed the onset of damage along the direction transverse to the fiber as compared to traditional CFRP. The CFRP composites with dispersed CNTs displayed slightly improved transverse modulus compared to the radially-grown architecture. The results also highlighted that the radially grown displayed better fracture properties than CFRP with dispersed CNT architecture. Thus, the developed high-fidelity computational framework can be further integrated with bottom-up multiscale modeling approaches that could serve as a useful tool to guide the design, development, and optimization of radially-grown CNT architectures with improved performance metrics at the structural length scale.

## Acknowledgment

This research is supported by the Office of Naval Research, Grant number: N00014-17-1-2037. The program manager is Mr. William Nickerson. The authors also acknowledge Dr. Anisur Rahman, a technical liaison for this research and the DoD ERDC Supercomputing Resource Center.

## References

[1] Erik T. Thostenson, Zhifeng Ren, Tsu-Wei Chou, Advances in the science and technology of carbon nanotubes and their composites: a review, Compos. Sci. Technol. 61 (13) (2001) 1899–1912.
[2] Siddhant Datta, Masoud Yekani Fard, Aditi Chattopadhyay, High-speed surfactant-free fabrication of large carbon nanotube membranes for multifunctional composites, J. Aero. Eng. 29 (3) (2015), 04015060.
[3] Siddhant Datta, Rajesh Kumar Neerukatti, Aditi Chattopadhyay, Buckypaper embedded self-sensing composite for real-time fatigue damage diagnosis and prognosis, Carbon 139 (2018) 353–360.
[4] Ashwin Rai, Siddhant Datta, Aditi Chattopadhyay, Carlos Lopez, Reinforcement of composite joint interface using nanomaterials, in: ASME 2017 International Mechanical Engineering Congress and Exposition, American Society of Mechanical Engineers, 2017. V009T12A002-V009T12A002.
[5] Keith J. Green, Derrick R. Dean, Uday K. Vaidya, Elijah Nyairo, Multiscale fiber reinforced composites based on a carbon nanofiber/epoxy nanophased polymer matrix: synthesis, mechanical, and thermomechanical behavior, Compos. Appl. Sci. Manuf. 40 (9) (2009) 1470–1475.
[6] William Frazier, Venkatesan Manivannan, Steven Fagan, Sean Field, Mark Hurley, Mike Allen, Mike McGonigle, Anisur Rahman, Dave Eby, Michael Block, Nano-enabled Technologies for Naval Aviation Applications, 2015. No. Nawcadpax/tim-2015/294. Naval air warfare center aircraft div patuxent river md.
[7] Emilie J. Siochi, Joycelyn S. Harrison, Structural nanocomposites for aerospace applications, MRS Bull. 40 (10) (2015) 829–835.
[8] C.R. Carpenter, P.H. Shipway, Y. Zhu, D.P. Weston, Effective dispersal of CNTs in the fabrication of electrodeposited nanocomposites, Surf. Coating. Technol. 205 (20) (2011) 4832–4837.
[9] H. Qian, A. Bismarck, E.S. Greenhalgh, G. Kalinka, M.S.P. Shaffer, Hierarchical composites reinforced with carbon nanotube grafted fibers: the potential assessed at the single fiber level, Chem. Mater. 20 (5) (2008) 1862–1869.
[10] C. Wang, Y. Li, L. Tong, Q. Song, K. Li, J. Li, et al., The role of grafting force and surface wettability in interfacial enhancement of carbon nanotube/carbon fiber hierarchical composites, Carbon 9 (2014) 239–246.
[11] C. Wang, Y. Li, L. Tong, Q. Song, K. Li, J. Li, et al., The role of grafting force and surface wettability in interfacial enhancement of carbon nanotube/carbon fiber hierarchical composites, Carbon 9 (2014) 239–246.
[12] Luman Zhang, Niels De Greef, Gerhard Kalinka, Bart Van Bilzen, Jean-Pierre Locquet, Ignaas Verpoest, Jin Won Seo, Carbon nanotube-grafted carbon fiber polymer composites: damage characterization on the micro-scale, Compos. B Eng. 126 (2017) 202–210.
[13] A.Y. Boroujeni, M. Tehrani, A.J. Nelson, M. Al-Haik, Hybrid carbon nanotubecarbon fiber composites with improved in-plane mechanical properties, Compos. B Eng. 66 (2014) 475–483.
[14] F.H. Zhang, R.G. Wang, X.D. He, C. Wang, L.N. Ren, Interfacial shearing strength and reinforcing mechanisms of an epoxy composite reinforced using a carbon nanotube/carbon fiber hybrid, J. Mater. Sci. 44 (2009) 3574–3577.
[15] Carlos Medina, Eduardo Fernandez, Alexis Salas, Fernando Naya, Jon Molina-Aldereguía, Manuel F. Melendrez, Paulo Flores, Multiscale characterization of nanoengineered fiber-reinforced composites: effect of carbon nanotubes on the out-of-plane mechanical behavior, J. Nanomater. 2017 (2017).
[16] H. Liu, L.C. Brinson, Reinforcing efficiency of nanoparticles: a simple comparison for polymer nanocomposites, Compos. Sci. Technol. 68 (2008) 1502–1512.
[17] G.D. Seidel, D.C. Lagoudas, Micromechanical analysis of the effective elastic properties of carbon nanotube reinforced composites, Mech. Mater. 38 (2006) 884–907.
[18] Roham Rafiee, Ghorbanhosseini Amin, Predicting mechanical properties of fuzzy fiber reinforced composites: radially grown carbon nanotubes on the carbon fiber, Int. J. Mech. Mater. Des. 14 (1) (2018) 37–50.
[19] P.K. Valavala, G.M. Odegard, E.C. Aifantis, Influence of representative volume element size on predicted elastic properties of polymer materials, Model. Simulat. Mater. Sci. Eng. 17 (4) (2009), 045004.
[20] Jihua Gou, Zhiyong Liang, Chuck Zhang, Ben Wang, Computational analysis of effect of single-walled carbon nanotube rope on molecular interaction and load transfer of nanocomposites, Compos. B Eng. 36 (6–7) (2005) 524–533.
[21] George Chatzigeorgiou, Gary Don Seidel, C. Dimitris, Lagoudas, Effective mechanical properties of “fuzzy fiber” composites, Compos. B Eng. 43 (6) (2012) 2577–2593.
[22] S.I. Kundalwal, M.C. Ray, Effective properties of a novel continuous fuzzy-fiber reinforced composite using the method of cells and the finite element method, Eur. J. Mech. Solid. 36 (2012) 191–203.
[23] S.I. Kundalwal, M.C. Ray, Micromechanical analysis of fuzzy fiber reinforced composites, Int. J. Mech. Mater. Des. 7 (2) (2011) 149–166.
[24] Rafiee, Roham, and Amin Ghorbanhosseini. "Predicting mechanical properties of fuzzy fiber reinforced composites: radially grown carbon nanotubes on the carbon fiber." Int. J. Mech. Mater. Des.: 1-14.
[25] Roham Rafiee, Ghorbanhosseini Amin, Stochastic multi-scale modeling of randomly grown CNTs on carbon fiber, Mech. Mater. 106 (2017) 1–7.
[26] Nithya Subramanian, Bonsung Koo, Karthik Rajan Venkatesan, Aditi Chattopadhyay, Computational analysis for the interface mechanics of carbon fibers with radially-grown carbon nanotubes, Carbon 134 (2018) 123–133.
[27] A. Rai, N. Subramanian, B. Koo, A. Chattopadhyay, Multiscale damage analysis of cnt nanocomposite using a continuum damage mechanics approach, J. Compos. Mater. 51 (6) (2017) 847–858.
[28] N. Subramanian, B. Koo, A. Rai, A. Chattopadhyay, A multiscale damage initiation model for cnt-ehanced epoxy polymers, in: 20th International Conference on Composite Materials. Copenhagen, Den-mark, 2013, pp. 4410–4418.
[29] W.L. Jorgensen, D.S. Maxwell, J. Tirado-Rives, Development and testing of the OPLS all-atom force field on conformational energetics and properties of organic liquids, J. Am. Chem. Soc. 118 (45) (1996) 11225–11236.
[30] J. Zang, Q. Yuan, F. Wang, A comparative study of Young's modulus of single-walled carbon nanotube by CPMD, MD and first principle simulations, Comput. Mater. Sci. 46 (3) (2009) 621–625.
[31] T.A. Halgren, Merck molecular force field. I. Basis, form, scope, parameterization, and performance of MMFF94, J. Comput. Chem. 17 (5-6) (1996) 490–519.
[32] S.K. Singh, S.G. Srinivasan, M. Neek-Amal, Thermal properties of fluorinated graphene, Phys. Rev. B 87 (10) (2013) 104114.
[33] A.K. Subramaniyan, C. Sun, Continuum interpretation of virial stress in molecular simulations, Int. J. Solid Struct. 45 (14) (2008) 4340–4346.
[34] Nithya Subramanian, Aditi Chattopadhyay, Molecular dynamics simulations for the analysis of nano-engineered fuzzy fiber composites, in: 2018 AIAA/AHS Adaptive Structures Conference, 2018, p. 1284.
[35] Nithya Subramanian, Ashwin Rai, Aditi Chattopadhyay, Atomistically informed stochastic multiscale model to predict the behavior of carbon nanotube-enhanced nanocomposites, Carbon 94 (2015) 661–672.
[36] Y.Y. Zhu, S. Cescotto, A fully coupled elasto-visco-plastic damage theory for anisotropic materials, Int. J. Solid Struct. 32 (11) (1995) 1607–1641.
[37] Mattias Olsson, Matti Ristinmaa, Damage evolution in elasto-plastic materials-material response due to different concepts, Int. J. Damage Mech. 12 (2) (2003) 115–139.
[38] Djordje Perić, On a class of constitutive equations in viscoplasticity: formulation and computational issues, Int. J. Numer. Methods Eng. 36 (8) (1993) 1365–1393.
[39] V.S. Romanov, S.V. Lomov, I. Verpoest, L. Gorbatikh, Modelling evidence of stress concentration mitigation at the micro-scale in polymer composites by the addition of carbon nanotubes, Carbon 82 (2015) 184–194.
[40] Jacob Aboudi, Marek-Jerzy Pindera, High-fidelity micromechanical modeling of continuously reinforced elastic multiphase materials undergoing finite deformations, Math. Mech. Solid 9 (6) (2004) 599–628.
[41] Ashwin Rai, Nithya Subramanian, Aditi Chattopadhyay, Investigation of damage mechanisms in CNT nanocomposites using multiscale analysis, Int. J. Solid Struct. 120 (2017) 115–124.
[42] Mandar Kulkarni, David Carnahan, Kapil Kulkarni, Qian Dong, L. Jandro, Abot, Elastic response of a carbon nanotube fiber reinforced polymeric composite: a numerical and experimental study, Compos. B Eng. 41 (5) (2010) 414–421.
[43] Richard Li, Noa Lachman, Peter Florin, H. Daniel Wagner, Brian L. Wardle, Hierarchical carbon nanotube carbon fiber unidirectional composites with preserved tensile and interfacial properties, Compos. Sci. Technol. 117 (2015) 139–145.
[44] Hui-Zu Shan, Tsu-Wei Chou, Transverse elastic moduli of unidirectional fiber composites with fiber/matrix interfacial debonding, Compos. Sci. Technol. 53 (4) (1995) 383–391.
[45] Sunny S. Wicks, Wennie Wang, Marcel R. Williams, Brian L. Wardle, Multi-scale interlaminar fracture mechanisms in woven composite laminates reinforced with aligned carbon nanotubes, Compos. Sci. Technol. 100 (2014) 128–135.